Full Winter Season Measurement of Snowpack Height and Backscattering Coefficient Using a 120-GHz Ultrawideband FMCW Radar

Víctor Herráiz-López, Adrián Subías Martín, Iñigo Salinas, Samuel T. Buisán, and Rafael Alonso

***Abstract*— In this article, we present a 120-GHz ultrawideband (3.3 GHz) frequency-modulated continuous wave (FMCW) radar, designed using a millimeter-wave (mmWave) transceiver, and its application to the measurement of snowpack height over two full winter seasons. This system achieves 2 cm accuracy across the diverse snowpack and environmental conditions encountered during the winter season. Its main advantages over conventional measurement techniques are good performance during heavy snowfall, correct detection of fresh fallen snow, spatial averaging, and low temperature dependence. Furthermore, our system is able to measure the backscattering coefficient of the snowpack, which is predominantly influenced by the liquid water content (LWC) of its surface layer. This relationship is confirmed by experimental measurements and numerical simulations, and could enable noninvasive first layer LWC estimations. Hence, we prove mmWave radar to be a reliable technology for snowpack monitoring under different environmental and snowpack conditions, with a wide range of applications in hydrological forecasting, avalanche risk assessment, and environmental monitoring.**

***Index Terms*— Frequency-modulated continuous wave (FMCW) radar, liquid water content (LWC), millimeter-wave (mmWave), snow backscattering, snow height, snow microstructure, snow thickness, snow wetness, thermal behavior, ultrawideband (UWB) radar.**

I. Introduction

SNOW plays an important role in the hydrological cycle in cold and mountainous areas, as well as in watersheds where it has a notable impact. It serves as a natural water reservoir during winter, gradually melting as temperatures rise, thereby increasing liquid water reserves and contributing to river flows [1], [2], [3], [4], [5]. Accurate assessment of snow reserves is, therefore, essential for hydrological forecasting and decision-making, not only in snow accumulation areas but also in downstream regions affected by snowmelt [6]. Moreover, the distribution, characteristics, and temporal evolution of the snowpack significantly impact various mountain processes and can undergo rapid changes throughout the winter season [7], [8], therefore requiring continuous, reliable, and real-time remote monitoring. This information is crucial for hydrological forecasting [9], environmental assessment [10], and avalanche risk evaluation [11].

Fig. 1. AEMET-Formigal field laboratory, located in the Spanish Pyrenees (42°45′41″N 0°23′32″W) at an elevation of 1800 m. This is the chosen location for the full winter season validation of the FMCW radar.

The snow-water equivalent (SWE), the amount of water contained within the snow, is one of the most important magnitudes for the characterization of the snowpack [12], [13]. A common method for measuring the SWE involves determining the snowpack height and its average density. As the snowpack is a multilayered structure, this requires the excavation of a snow pit deep enough to account for the different possible densities [14]. However, this is a destructive technique that needs human intervention and is not valid for continuous monitoring of the SWE.

Among the noninvasive techniques, which generally allow this continuous measurement, we can find several options, like pressure and load cells, techniques relying on the changes of the dielectric properties of the snowpack with density [15], measurement of the attenuation of cosmic-ray neutrons by the snowpack [16], radar techniques relying on the propagation of electromagnetic radiation emitted by an active sensor above the snowpack [17], [18], [19], and estimation of Global Positioning System (GPS) signals attenuation and time delay [20].

Regarding the measurement of snowpack height, the simplest techniques involve conducting in situ manual measurements requiring human intervention. However, there is a limited variety of options for automated and noninvasive

Received 20 December 2024; revised 13 May 2025; accepted 26 June 2025. Date of publication 2 July 2025; date of current version 11 July 2025. This work was supported in part by MCIN/AEI/10.13039/501100011033 and the European Union (EU/FEDER) through joint funding of projects (NextGenerationEU/PRTR) under Grant PID2021-124451OB-I00 and Grant TED2021-131180B-I00 and in part by the Research Project funded by DGA-FSE under Grant T20-23R. *(Corresponding author: Víctor Herráiz-López.)*

Víctor Herráiz-López, Adrián Subías Martín, and Rafael Alonso are with the Departamento de Física Aplicada, Universidad de Zaragoza, 50009 Zaragoza, Spain (e-mail: vherraiz@unizar.es).

Iñigo Salinas is with the Departamento de Ingeniería Electrónica y Comunicaciones, Universidad de Zaragoza, 50018 Zaragoza, Spain.

Samuel T. Buisán is with the Delegación Territorial de AEMET (Spanish State Meteorological Agency) en Aragón, 50007 Zaragoza, Spain.

Digital Object Identifier 10.1109/TGRS.2025.3585426

measurement of the snowpack height. Radar methods based on the measurement of the time-of-flight (ToF) of a pulse propagating from the snowpack surface to the ground are sometimes employed [21], [22]. These techniques require prior knowledge of the propagation speed of light within the snowpack, which is strongly influenced by its density and liquid water content (LWC) [23], [24], [25], [26], thus limiting their potential accuracy. Consequently, many techniques rely on the installation of a fixed structure housing a distance measurement device to estimate the distance between the device itself and the snow cover surface. By determining the distance from the device to the ground, typically measured in the absence of snow cover, the height of the snowpack can be easily calculated [15].

The distance measurement device typically employs either a laser or an ultrasonic ToF sensor, both of which have certain limitations. For example, the low acoustic impedance of fresh snow [27], [28] can result in noisy measurements from ultrasonic sensors. Additionally, these sensors are highly sensitive to environmental conditions, which can hinder their performance during intense snowfall and strong wind periods [29]. In the case of laser sensors, their small spot size and the snowpack heterogeneity require the use of mechanical components to average the measurement of nearby points [30]. Mechanical components increase the cost of the sensor and complicate its maintenance, which is a major drawback in remote inaccessible areas. In this context, the use of a millimeter-wave (mmWave) radar sensor has been proposed as an alternative to measure snowpack height [31], [32]; however, no systematic studies have yet been reported on its performance under different snowpack and environmental conditions.

The rapid advancement of mmWave technology in recent years has led to the development of reliable, low-cost devices capable of both generating and detecting this range of electromagnetic radiation [33], [34]. Given that the size of ice crystals within the snowpack is comparable to the wavelength of mmWave radiation, significant scattering occurs under most snowpack conditions. Also, the field of view of mmWave sensors can be adjusted using reflectors or dielectric lenses, thus controlling the spot size as an averaging mechanism. These kind of devices have low power requirements, and can function even under harsh environmental conditions, as heavy snowfall, and the propagation speed of mmWave radiation in air is weakly affected by environmental factors. As a result, mmWave technology could potentially solve many of the problems of commercial snowpack height measurement devices and complement their use in locations where its advantages are valuable.

In this work, we will present a prototype snowpack height sensor based on a low-cost 120-GHz in-phase and quadrature (I/Q) transceiver chip, which enables the design of a frequency-modulated continuous wave (FMCW) radar sensor using low-cost electronics. We will demonstrate its viability comparing data collected over two full winter seasons to measurements from a laser gauging device and in situ manual observations, validating its performance in a wide range of environmental and snowpack conditions. We will also address the effect of snowpack features on radar performance, as this understanding is essential for conducting a comprehensive seasonal analysis. Once the mmWave-snowpack interaction is understood, we will discuss the potential of the proposed sensor for the inference of snowpack surface LWC.

Field measurements have been performed at the AEMET-Formigal field laboratory (see Fig. 1), located on a small plateau in the Spanish Pyrenees (42° 45′ 41″N, 0° 23′ 32″W) at an elevation of 1800 m above sea level. This site was the location established by the Spanish Meteorology Agency (Agencia Estatal de Meteorología, AEMET) to participate in the World Meteorological Organization Solid Precipitation Intercomparison Experiment (WMO-SPICE) [35], [36], [37]. Snowfalls are frequent, with an average maximum snowpack height of 1.7 m in recent years, and peak accumulations exceeding 3 m during certain winter seasons. The snow cover remains highly homogeneous in the experimental area due to its low exposure to the wind. The AEMET-Formigal field laboratory is an excellent location for testing snowpack height sensors, as it provides a wide range of environmental and snowpack conditions over the course of a winter season.

The rest of the document is organized as follows. In Section II, we present the radar system, including hardware design, data processing and analysis, and laboratory calibration. Section III contains the results of the continuous measurement of the snowpack height during a full winter season and their comparation to other measurement techniques. Section IV includes the measurement of the snowpack backscattering coefficient using the radar system and its potential application to the estimation of the snowpack surface LWC. Finally, Section V lays down the main results and conclusions from this work.

II. 120-GHz FMCW Radar System

The basis of a radar system is the use of electromagnetic radiation to obtain information about the position, or speed, of a certain object [38]. While pulsed radars are more common in long-range applications, short-range measurements frequently use FMCW radars, which allow simultaneous measurement of position and speed of multiple targets [39], [40]. Our system is based on a mmWave transceiver manufactured by Indie Semiconductor, and the I/Q transceiver TRX_120_067 [41], as the core of a 120 −GHz ($\lambda = 2.5$ mm) FMCW radar. A schematic of the transceiver is included in Fig. 2(a). It offers a maximum bandwidth of 6.3 GHz, an output power of −3 dBm, low power consumption (380 mW in continuous operating mode, supplied through a single 3.3 V source), and performs up and down-conversion of both the generated and detected signals. It is encapsulated in an 8×8 mm^2 package which contains, apart from the generation and detection electronics, amplifying stages and the transmitting (TX) and receiving (RX) antennas, with around 8 dBi gain in the working frequency band. As the up/down-conversion is performed at the transceiver, the system requires only low-frequency (LF) electronics for the control of the frequency of the generated signal and for signal detection. High-accuracy range measurements under laboratory conditions have been

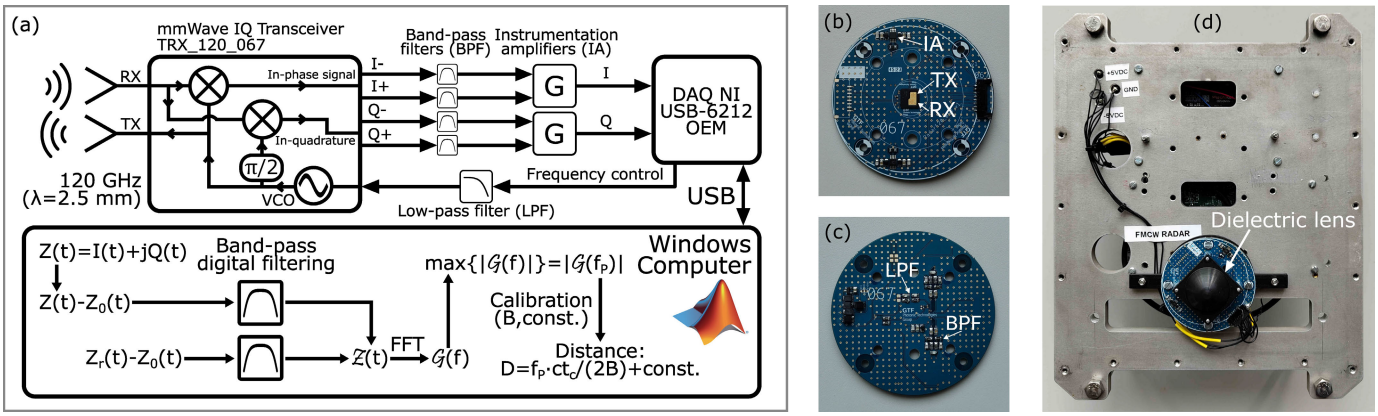

Fig. 2. (a) Block diagram of the FMCW radar sensor including the mmWave transceiver, the analog input and output conditioning stages, and the main signal processing steps. (b) (Top) Layer of the radar PCB, with the 120 GHz transceiver in the center of the board and the IAs. (Diameter: 70 mm). (c) (Bottom) Layer of the PCB, with the input and output filtering stages and the supply circuits. (d) FMCW radar sensor with the dielectric lens mounted on an aluminum plate.

reported in recent years using these kind of modules [42], [43], [44], [45], [46]. In this study, the FMCW radar uses a frequency chirp with a span of $B = 3.3$ GHz centered at a frequency of 122.5 GHz. Each measurement consists on the average of 300 chirps of a duration $t_c = 10.24$ ms, separated by 5 ms pauses. Since the snowpack is a static object, the total duration of the measurement and of each chirp is not a critical parameter.

Fig. 2(b) and (c) shows the printed circuit board (PCB) designed to hold the mmWave transceiver and the supply and signal conditioning stages, which are detailed in Fig. 2(a). The control and data acquisition (DAQ) are performed using a DAQ system from National Instruments (DAQ NI USB-6212 OEM). The carrier frequency is controlled inside the mmWave transceiver by a voltage-controlled oscillator (VCO), whose nonlinear dependence is compensated at the DAQ stage. The frequency-controlling signal is filtered by a second-order low-pass RC filter (LPF) [43], [46] with a cut-off frequency of 50 kHz to reduce its noise. The I/Q components generated by the transceiver are bandpass filtered using a second-order RC filter (BPF, cut-off frequencies of 2.2 and 16 kHz). Then, they are amplified using an instrumentation amplifier (IA) with a gain of $G = 100$, ensuring optimal use of the input range of the DAQ system. To increase the measurement range and control, the sensor field of view we have employed an Indie Semiconductor dielectric collimator lens [Fig. 2(d)] which provides about 40 dB emission and detection gains [47].

The analog to digital conversion of the down-converted input signals is performed using a sampling frequency of 200 kHz, resulting in 2048 samples for each chirp period. As the radar will deal with static objects, we can select a relatively slow chirp time to measure the snowpack height, thus improving the signal-to-noise ratio (SNR). Using 300 chirps averaging also improves the SNR by reducing the random noise. Multitarget resolution increases with chirp bandwidth, so the selected bandwidth will be the maximum possible one without causing linearity issues. The cut-off frequencies of the bandpass filters are chosen to filter out signals from distances smaller than 1 m and over 7.5 m. The pause time between chirps ensures the complete relaxation of the RC filter.

Fig. 3. (Bottom left) FMCW radar sensor installed at the AEMET-Formigal field laboratory. The sensor is housed within a protective plastic radome.

The radar system formed by the PCB, the DAQ, and a Windows-based computer (LattePanda Alpha) is mounted on an aluminum plate protected by plastic radomes. In Fig. 2(a) we show a block diagram of the FMCW radar sensor, detailing its analog filtering and amplifying stages, and an schematic of the digital data processing, which will be detailed in the following section.

Fig. 2(d) shows the aluminum plate holding the complete radar system. We have developed protective radomes, crafted by 3-D printing with PLA, then waterproofed and painted for enhanced durability. These radomes allow the FMCW radar to operate under harsh environmental conditions, as heavy snowfall periods. Fig. 3 shows the prototype, with the plastic radomes, installed at the AEMET-Formigal field laboratory. The introduction of the radomes produces a reflection of the radar signal close to the source and thus a LF component in the FMCW trace, which will be rejected by the bandpass filter. This results in an additional 8 dB of attenuation for the signal from the snowpack. The final SNR of the system with the radome is approximately 40 dB.

A. Radar System Calibration

We validated the correct operation under laboratory conditions of the radar sensor using a metal reflector placed at different distances. The measurements presented here are the

average of 50 consecutive chirps, separated by 5 ms pauses. In the field experiments, the averaging was performed over 300 chirps.

The signal $Z(t) = I(t) + jQ(t)$ produced by a single target at a distance R can be expressed as [48]

$$Z(t) = Z_0(t) + A(t)\alpha(R)\exp\left[2\pi j(f_b t - f_0\tau)\right] \quad (1)$$

where $f_b = 2BR/(ct_c)$ is the beat frequency, $\alpha(R)$ accounts for the reflection properties of the object and the attenuation in the round-trip, f_0 is the starting frequency of the chirp pulse, $\tau = 2R/c$, and c is the speed of light in vacuum. $Z_0(t)$ is the background signal (which includes clutter due to the radome and the direct coupling between the antennas) and $A(t)$ is a time modulation produced by the transmitter and receiver dependence on frequency. Equation (1) does not account for spectral components at negative frequencies, caused by IQ imbalance in the transceiver [42], nor for multiple reflections between the snowpack and the measurement device, as these effects will be eliminated on the digital filtering stage.

Measuring the background signal $Z_0(t)$ in the absence of any object and using a reference measurement, $Z_r(t)$ taken with the metal reflector located at a known distance R_r, according to [48] we define our signal of interest as [see Fig. 2(a)]

$$\mathcal{Z}(t) = \frac{Z(t) - Z_0(t)}{Z_r(t) - Z_0(t)}. \quad (2)$$

This established calibration procedure improves the accuracy of short-range FMCW radar systems [49], [50], compensating the effects of clutter and time modulation. As a side effect, this definition produces a frequency shift that can even generate negative frequency components. However, this shift can be calibrated, as performed in Fig. 4, and does not affect the accuracy of the measurements.

The reference signal $Z_r(t)$ is a measurement of a metal reflector at a distance of 1.464 m. It has been filtered, after the subtraction of $Z_0(t)$, using a bandpass finite impulse response (FIR) filter with cut-off frequencies of 1.7 and 4.4 kHz. As the distance range from the sensor to the snow cover in the field location is known, we can also filter the signal on the numerator of (2) using another bandpass FIR filter with cut-off frequencies of 1 and 9 kHz.

Fig. 4(a) shows the spectrum, $\mathcal{G}(f) = \mathrm{FT}[\mathcal{Z}(t)]$, of the measurements of a metal reflector placed at different distances from the radar. The frequency of the maximum peak, f_P, is related to the position of the metal reflector. In Fig. 4(b), we confirm the expected linear relation between the peak frequency and the distance between sensor and reflector. The linear fit of these measurements allows us to calculate the real bandwidth of the chirp as 3.3 GHz. Although we are not using the complete bandwidth offered by the mmWave transceiver due to limitations introduced by the filtering stages (both analogical and digital), the drawback is only a smaller multitarget accuracy, which is not critical for our application.

Sub-millimetric accuracy has been reported under laboratory conditions using mmWave radar technologies (see, e.g., [51]). However, the accuracy of our radar sensor will be reduced on site due to noise and temperature drifts, resulting in centimetric precision. Nevertheless, this level of precision is sufficient for measuring snowpack height, as its surface roughness is often on the order of centimeters.

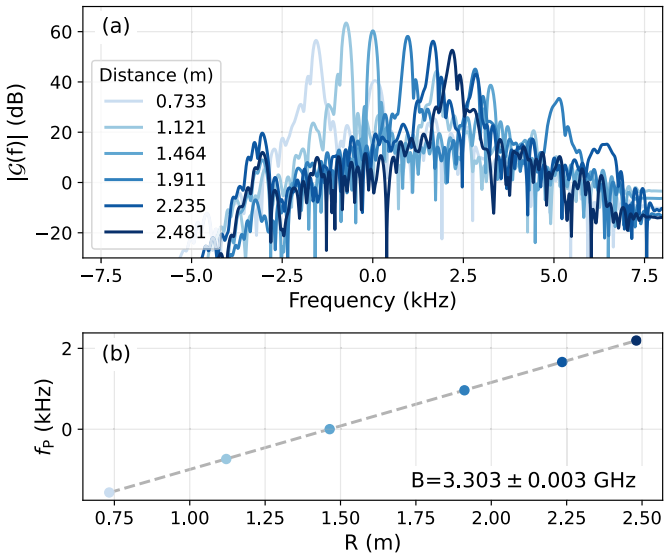

Fig. 4. (a) FMCW spectrum of a metal reflector at different distances from the radar, corrected using (2). (b) Linear relation between the peak frequency of the spectrum (f_P) and the distance to the metal reflector, R.

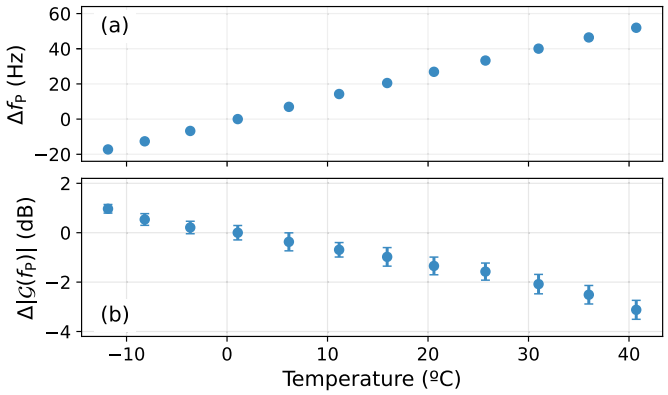

Fig. 5. (a) Thermal behavior of the peak frequency of the corrected spectrum. (b) Thermal behavior of the amplitude at the maximum of the corrected spectrum. Both magnitudes are referenced to the value at 0 °C.

B. Thermal Behavior

To analyze the influence of the working temperature, the radar system has been characterized using a thermal chamber. Placing a single object in the field of view of the radar at a distance of about 55 cm, we can measure the dependence of the frequency and amplitude of the FMCW signal with temperature. In Fig. 5, we show the variation in the amplitude and frequency of the main spectral component of the corrected signals. At each temperature, we performed 100 different measurements consisting on the average of 300 consecutive chirps.

Fig. 5(a) shows a frequency shift of 69 Hz across a temperature range of 55 °C, which is caused by an increase of the effective bandwidth as temperature increases. Using the

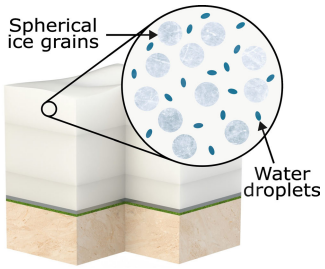

Fig. 6. Sketch of the microstructure model for the computation of the scattering and absorption properties of the snowpack. The spherical ice grains and the ellipsoidal water inclusions are surrounded by air.

calibration from Fig. 4 without compensation, the apparent position shift is 3.2 cm across the whole temperature range.

Fig. 5(b) shows a change of −4.1 dB in the amplitude of the detected signal over the 55 °C tested range. It is caused by a variation not only in the power emitted by the mmWave transceiver [41], but also in the receiver efficiency. As the radar system gets warmer, it emits less power, but also the standard deviation of the different measurements increases.

In Section III, these temperature effects in the measurement of snowpack height will not be compensated, as the accuracy obtained is good enough. However, in Section IV, they will be taken into account, as the amplitude of the spectral components is key to the study of the snowpack backscattering.

C. mmWave Interaction With the Snowpack

Understanding the mmWave-snowpack interaction is crucial to the design and calibration of the radar sensor. Scattering plays an important role in this interaction, as the mmWave wavelength is comparable to the size of the ice crystals in snow. Hence, we will need to take into account not only the electromagnetic properties of the snowpack constituents (mainly ice, liquid water, and air), but also its microstructure, as it plays a critical role in the scattering phenomena.

The electromagnetic properties of ice and water will be based on the models presented in [52, Ch. 4]. The electromagnetic behavior of water in its solid and liquid phases differs significantly at 120 GHz, as shown by their respective penetration depth values (the distance at which the intensity of a propagating wave is decreased by a factor $1/e$). This depth is 6.4 cm for pure ice and 0.15 mm for liquid water [52, Ch. 4]. This difference arises due to the existence of a rotational mode in the water molecule, which increases the absorption of mmWaves by liquid water compared to ice (and the absorption by wet snow compared to dry snow).

The microstructure of snow will be described using a model common in both microwave and mmWave remote sensing [52], [53], [54], which is outlined in Fig. 6. We consider snow to be formed by air and ice spheres, which mainly determine the scattering behavior, and smaller ellipsoidal water inclusions, which do not produce significant scattering but play an important role in the absorption properties. This model is thus determined by the radius of the ice spheres and the volumetric fractions of ice and liquid water.

In dense media, where scattering centers occupy an appreciable fraction of the total volume, the radiative transfer equation (RTE) is commonly used to explain the scattering of electromagnetic radiation. The scalar RTE is given by

$$\frac{dI\left(\vec{r},\hat{s}\right)}{ds} = -\kappa_{\mathrm{e}} I\left(\vec{r},\hat{s}\right) + \int\int_{4\pi} \Psi\left(\hat{s},\hat{s}'\right) I\left(\vec{r},\hat{s}'\right) d\Omega' \quad (3)$$

where $I(\vec{r},\hat{s})$ is the intensity of the electromagnetic wave propagating in the direction of $\hat{s}$ at a point $\vec{r}$, κ_{e} is the extinction coefficient, and $\Psi(\hat{s},\hat{s}')$ describes how the radiation propagating in the direction $\hat{s}'$ is scattered into the direction $\hat{s}$. Both κ_{e} and $\Psi(\hat{s},\hat{s}')$ are determined by the scattering properties of the snowpack (which generally vary along the vertical profile). As the scattering ice particles are considered spherical and we will assume incidence normal to the snowpack, we can employ the scalar RTE. Although the use of the RTE for the snowpack with mmWave coherent emitters may seem inappropriate, it is widely spread and the comparison to experimental measurements is satisfactory [54], [55], [56], [57], due to the fact that ice particles are, approximately, randomly located.

The extinction coefficient from (3) describes the exponential decay suffered by a beam propagating through a scattering and/or absorbent medium. It is directly related to the penetration depth of the radiation δ_p

$$\delta_p = 1/\kappa_{\mathrm{e}} \,. \quad (4)$$

As will be shown in Section IV, the penetration depth of the 120 GHz electromagnetic radiation in wet snow is limited to a few millimeters due to absorption. However, in dry snow conditions, this depth can increase to several centimeters. Also, the penetration depth of snow is smaller than that of ice, mainly because of scattering.

III. Field Measurements of the Snowpack Height During the 2023–2024 and 2024–2025 Winter Seasons

We performed a continuous measurement of the snowpack height in the AEMET-Formigal field laboratory during two consecutive winter seasons. In the 2023–2024 season, the measurements started in February, when snow started accumulating in the region after the complete melting of the previous snow cover, until May, when the snow cover completely disappeared from the experimental area. The measurement interval was 5 min, except for periods of intense snowfall when it was reduced to 3 min. The total number of measurements during this winter season was 26 972. After discarding the measurements with too low SNR, the final number was 22 726. Using the process described in Section II, we can obtain the distance between the radar and the snowpack surface with the maximum of the FMCW spectrum. As the distance between the radar and the soil surface is known, we can then easily obtain the snowpack height, following the same procedure of laser and ultrasonic sensors.

In the 2024–2025 winter, the measurements expand from December to May in 10 min intervals. The intervals were longer this time, as the accuracy obtained was comparable. In total, there are 17 731 measurements, and 15 229 after discarding those with low SNR.

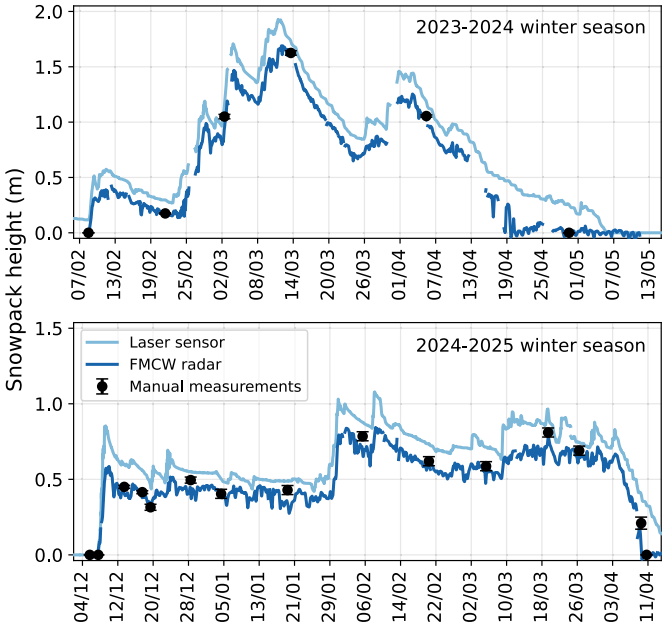

Fig. 7. Snowpack height in the experimental area measured by our FMCW radar, a laser sensor Lufft SHM 31 (installed at a slightly different location, causing the approximately constant height difference), and an avalanche probe (in situ manual measurements taken directly beneath the radar sensor).

In Fig. 7, we show the measured snowpack height using the FMCW radar sensor, smoothed with local linear regression to reduce noise in the time series. The local linear regression is performed over a 5-h window centered on the point under consideration for the 2023–2024 winter season, and over a 10-h window for the 2024–2025 winter season. The time window has been changed to preserve the number of measurements included in the linear regression. These measurements are compared to the snowpack height in the experimental area as reported by a laser sensor (Lufft SHM 31) placed at a distance of 5 m from our radar sensor. We also include several in situ manual measurements performed at the same location of the radar using an avalanche probe. The periods during which no measurements are available in the 2023–2024 season were caused by interruptions in the power supply of the experimental test-site, but are not related to the mmWave sensor itself. We consider the distance between radar and soil surface as the average of the measurements from May first in 2023–2024 winter season, as the snow cover had completely disappeared of the experimental area by then.

The radar and laser sensor measurements follow the same trend, confirming that our system is capable of measuring the snowpack height under different snowpack and environmental conditions, including extremely severe conditions as heavy snowfalls. However, there is a roughly constant offset between the two time series. It is caused by the roughness of the soil surface, which causes differences in the snowpack height under each sensor, as they are horizontally separated. This is reinforced by the manual measurements performed under the radar sensor, which confirm its the accuracy. The accuracy of the laser sensor was also verified separately.

Fig. 7 presents the main result of this article, demonstrating the feasibility of measuring the snowpack height in the different conditions found along two separate full winter seasons. We estimate the precision of the measurement in around 2 cm using the standard deviation of the measurements from May first in the 2023–2024 winter season, when the snow cover had already disappeared and the measured distance was that of the soil surface. Precision is mainly limited by the thermal drift of the mmWave transceiver presented in Fig. 5, so it could be increased by correcting this. However, centimeter-level precision is sufficient for most practical purposes when measuring snow depth, as the snowpack surface roughness is typically in the same order of magnitude.

IV. Snowpack Backscattering Coefficient: Influence of the Surface LWC

In the previous section, we have shown the possibility of measuring the snowpack height using the frequency of the major component of the FMCW signal spectrum. From the amplitude of that spectral component, we can also obtain information about the electromagnetic intensity of the wave backscattered from the snowpack. As the backscattering properties of mmWaves in the snowpack mainly depend on the physical properties of its surface, this measurement could be very useful for extracting information about these properties.

The snowpack is a distributed target, so we will define its backscattering coefficient (backscattering cross section per unit area) as [52, Ch. 5]

$$\sigma^0 = 4\pi R^2 \frac{\mathcal{I}_B}{\mathcal{I}_I} \frac{1}{A} \tag{5}$$

where $\mathcal{I}_I$ is the intensity of the electromagnetic wave incident at the object position, $\mathcal{I}_B$ is the intensity of the backscattered wave at the radar position, R is the distance between snowpack surface and radar, and A is the transverse section illuminated by the radar.

In this section, we will show that the mmWave backscattering coefficient is strongly affected by the snowpack surface properties. We will present a method for obtaining the backscattering coefficient from experimental FMCW radar measurements and from numerical simulation of the physical snowpack parameters, solving the RTE, (3). The intercomparison of measurements and electromagnetic simulation will help us understand the effect of the different snowpack parameters on the scattering coefficient, paving the way for the use of the radar sensor to measure snowpack surface properties, in addition to its geometrical height.

We will restrict our analysis of the backscattering coefficient to the period of time between March 17 and March 23 of the 2023–2024 winter season, during which the snowpack height gradually decreased after an intense snowfall period, as can be seen in Fig. 7. This height reduction was favored by warm temperatures and an intense solar radiation, as can be seen in Fig. 8(a) and (b), which also caused the appearance of liquid water in the upper layers of the snowpack. We have chosen this period of time because it is the largest in which the moderate temperatures and the absence of snowfalls result in the existence of liquid water in the snowpack surface. The major effect of the increase in the LWC is a much higher absorption of the electromagnetic radiation, thus decreasing

the penetration depth to the order of 1 mm. Additionally, the increase in LWC also reduces the single-scattering albedo, $0 \leq a \leq 1$, which accounts for the relative importance of the scattering and absorption phenomena in the snowpack. If $a \approx 0$, scattering is negligible compared to absorption, whereas for $a \approx 1$, scattering dominates. The combination of both effects allow us to simplify the resolution of the RTE.

A. Experimental Measurement of the Backscattering Coefficient

We can obtain the backscattering coefficient of the snowpack from the FMCW radar measurements by applying (5) after some considerations about the involved magnitudes. The illuminated area will depend on the distance between the snowpack and the radar as $A \propto R^2$, with the proportionality constant fixed by the field of view of the sensor. According to basic radar equations, the incident intensity follows $\mathcal{I}_I \propto K_1^2(T)R^{-2}$, where $K_1(T)$ is a temperature-dependent function which accounts for variations in the amplitude of the emitted electric field caused by temperature [41] and the proportionality constant depends on the TX antenna and dielectric lens gains, among other factors.

Additionally, we can express the backscattered electric field at the RX antenna, after using the signal-correcting procedure described in Section II, as

$$E_B(t) \propto \mathrm{Re}\left[K_2(T)\mathcal{Z}(t)e^{2\pi j\,\phi(t)}\right] \tag{6}$$

where $\phi(t) = f_0 t + Bt^2/(2t_c)$ is the phase of the transmitted FMCW signal, $K_2(T)$ is a temperature-dependent function which accounts for the variations in the detection efficiency caused by temperature and Re() denotes the real part of a complex quantity. For $K_1(T)$ and $K_2(T)$, we have to consider the operating temperature of the chip. Although their values have not been measured separately, their combined effect was measured in the thermal characterization of Section II. The backscattered intensity $\mathcal{I}_B$, measured at the RX antenna, is then given by

$$\mathcal{I}_B \propto \langle E_B^2(t)\rangle \propto K_2^2(T)\langle|\mathcal{Z}(t)|^2\rangle = \frac{K_2^2(T)}{t_c}\int_0^{t_c}|\mathcal{Z}(t)|^2\,dt \tag{7}$$

which using Parseval's Theorem can be expressed as

$$\mathcal{I}_B \propto K_2^2(T)\int_{-\infty}^{+\infty}|\mathcal{G}(f)|^2\,df \quad . \tag{8}$$

Hence, using the corrected spectrum and the distance between the radar and the snow surface, we can compute the backscattering coefficient of the snowpack as

$$\sigma^0 \propto \frac{K_1^2(T)}{K_2^2(T)}R^2\int_{-\infty}^{+\infty}|\mathcal{G}(f)|^2\,df \quad . \tag{9}$$

The temperature dependence of the efficiency factor can be obtained from Fig. 5, as $K_2^2(T)/K_1^2(T) \propto 1/\Delta|\mathcal{G}(f_\mathrm{P})|^2$. The ambient temperature in the field laboratory and the temperature inside another setup placed next to the radar sensor were constantly monitored during the winter season. This setup temperature is more appropriate to estimate the operating temperature of the radar, as it accounts for warming caused by solar radiance on the radome.

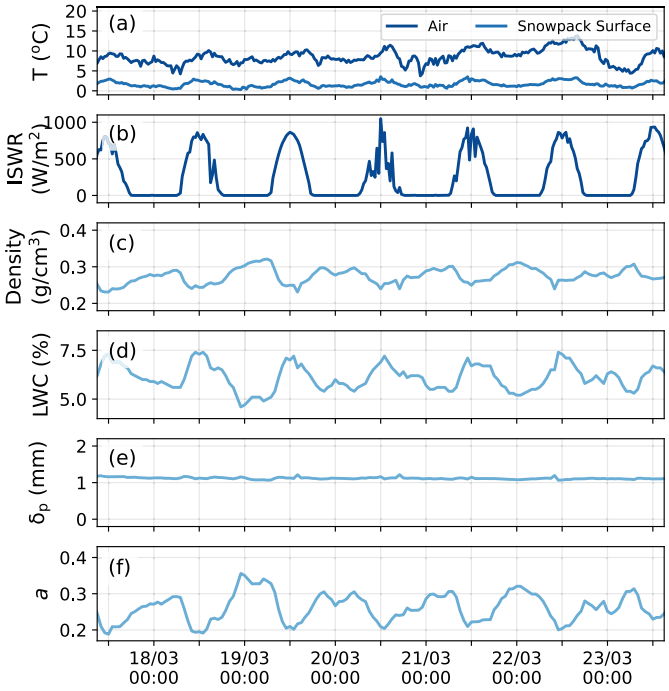

Fig. 8. Environmental variables measured at the field laboratory. (a) Snowpack surface and air temperatures and (b) incident shortwave radiation. Physical properties of the uppermost layer of the snowpack simulated using the software SNOWPACK. (c) Density and (d) LWC. Propagation properties of this snowpack layer, computed using the microstructure model of the snowpack. (e) Penetration depth and (f) single-scattering albedo.

B. Electromagnetic Simulation of the Backscattering Coefficient

Given the physical properties of the snowpack, the microstructure model from [52, Ch. 11], sketched in Fig. 6, allows the calculation of the propagation and scattering parameters required by the RTE. However, a general analytical solution to the RTE does not exist, and solving it numerically generally becomes a difficult task [53], [54], [56]. This is the main reason why we have restricted the calculations to the period from March 17 to March 23, when an approximate solution of the RTE can be applied. A penetration depth in the millimeter range makes it possible to consider the snowpack as a semi-infinite medium with homogeneous properties, simplifying the spatial dependence in the RTE. Additionally, when the single-scattering albedo is weak enough, that is $a \lesssim 0.3$ [52, Ch. 11], we can solve the RTE using an iterative method.

In Fig. 8(c) and (d), we show the density and LWC of the upper layer of the snowpack during the analyzed period, calculated using the SNOWPACK software, developed by the Swiss Federal Institute for Snow and Avalanche Research (SLF) [58], [59]. We used SNOWPACK to simulate the physical properties of the snowpack during the complete winter season in the experimental area. This allows us to evaluate different properties of the snow along its vertical profile, as its density, LWC, grain type, or temperature. SNOWPACK performs a simulation of the evolution of the snowpack physical parameters, modeling it as a 1-D layered system and using meteorological data (air temperature, relative humidity, wind speed, incoming short- and long-wave

radiation, reflected short wave radiation, snowpack surface temperature, precipitation, and soil temperature). Apart from density and LWC simulated by SNOWPACK, we have considered a constant ice grain diameter of 1 mm, justified by the absence of snowfall during the analyzed interval. This causes the snowpack surface to be formed by melt form grains [12] which undergo melting-refreezing cycles. A constant grain size has already been considered in previous studies, such as in [60].

From those three physical parameters, we can compute the scattering and propagation properties of the uppermost layer of the snowpack using the microstructure model. Fig. 8(e) shows the evolution of the penetration depth, which remains roughly constant at about 1 mm. Because of this millimeter penetration depth, the snowpack can be considered as a semi-infinite medium with homogeneous properties (equal to the properties of the uppermost layer). This is not possible under dry snow conditions, when the penetration depth can reach some centimeters. Fig. 8(f) shows the simulated single-scattering albedo of the uppermost layer, which meets the $a \lesssim 0.3$ criterion [52, Ch. 6] for the use of the iterative solution of the RTE in the semi-infinite medium. We can clearly see that the single-scattering albedo is strongly influenced by the day–night cycles predicted by SNOWPACK in the LWC of the snowpack surface (melting–refreezing cycles).

Although the density of the snowpack surface is also affected by day–night cycles, the shape of the variations is slightly different from that observed in the LWC and single-scattering albedo. The absence of clear day–night cycles in the penetration depth is due to it being affected by two opposing effects: during the day, the LWC increases, which produces higher absorption of radiation but reduces scattering. These effects partially counteract each other, resulting in a roughly constant penetration depth.

The aim of the simulation of the backscattering coefficient is to evaluate how it is affected by the different physical parameters of the snowpack. Hence, we do not seek to accurately solve the RTE but to obtain an intuitive and simple approximate solution to understand the measurements. It is in this context where we have decided to approximately solve the RTE using the single-scattering model, including only the first order of the iterative solution of the RTE. Under this approximation, the backscattering coefficient of the snowpack at normal incidence can be computed as [52, Ch. 11]

$$\sigma^0 = \frac{\kappa_b}{2\kappa_e} \tag{10}$$

where κ_e and κ_b are, respectively, the extinction and backscattering coefficients of the snowpack. Both can be obtained with the microstructure model in Fig. 6. We have not considered the scattering produced by the roughness of the snowpack surface, as it is negligible compared to the volumetric contribution. In Fig. 9, we show the simulated backscattering coefficient, computed using (10), which is mainly influenced by the day–night cycles in the LWC and single-scattering albedo (see Fig. 8).

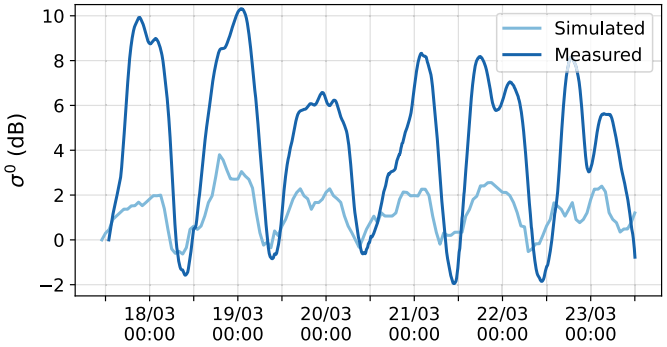

Fig. 9. Measured and simulated backscattering coefficient of the snowpack during the analyzed period. Measurements have been corrected according to the thermal behavior of the radar system.

C. Comparison of Measured and Simulated Values of the Backscattering Coefficient

Fig. 9 shows the intercomparison between the measured and simulated backscattering coefficient of the snowpack. Both time series have been normalized using its first value as a reference (0 dB). We can see the appearance of day–night cycles in the backscattering cross-section evolution. This had been previously reported at other frequency ranges both for the snowpack scattering properties and for its brightness temperature [55], [57], [60].

Comparing the temporal dependence in Figs. 8 and 9, we can see that the simulated backscattering coefficient is mainly influenced by the LWC, in the same way as the single-scattering albedo is. During the day, the increasing temperatures and the solar radiance produce the partial melting of ice crystals in the snowpack uppermost layer, increasing its LWC. The increase in the amount of liquid water intensifies the absorption of mmWaves by the snowpack and reduces its scattering (as the dielectric constant of the effective background medium from the microstructure model increases), resulting in a smaller backscattered intensity. On the contrary, the absence of solar radiance and lower temperature during the night cause the partial disappearance of liquid water, increasing again the backscattering coefficient of the snowpack, which usually reaches its daily maximum before sunrise.

Fig. 9 shows that those day–night cycles predicted by the numerical simulation are also observed in the FMCW radar measurements. The experimental measurements have been corrected using the temperature measured in a setup placed next to it using a Campbell datalogger model CR-300. However, the daily variation of the backscattering coefficient is larger in the experiment than in the simulation, and this difference cannot be explained by inaccuracies in the operating temperature estimation.

This difference can be caused by multiple factors, first among them the use of an approximate solution of the RTE. The single-scattering model does not account for processes consisting on consecutive scattering events contributing to the total backscattering, thus underestimating the backscattering coefficient. The single-scattering approximation becomes more precise as the albedo diminishes during the day, because the $a \lesssim 0.3$ criterion [52, Ch. 6] is met with a greater margin.

Additionally, the accuracy of the numerical simulation of the snowpack parameters can have a significant impact on the values for the simulated backscattering coefficient.

Although the single-scattering model does not provide accurate values, as expected due to the use of an approximate method for the solution of the RTE, it does confirm the temporal variation of the backscattering coefficient of the snowpack and its origin on the variation of the LWC in the uppermost snowpack layer. However, the numerical prediction of the backscattering coefficient could be improved by using a more complex microstructure model and a more precise solution for the RTE, as in [57]. This could eventually lead to the prediction of the backscattering coefficient from the physical snowpack properties with much greater accuracy, as already reported in other frequency ranges [55], [57]. Inverting this relation, we could even obtain a good approximation for the LWC of the uppermost snowpack layer from its backscattering coefficient, as the LWC is the variable with the largest influence on the scattering properties. This would open the possibility of employing a low-cost radar not only as a height sensor, but also as a nonperturbative measurement system for the LWC of the snowpack surface.

V. Conclusion

We have developed a prototype of a snowpack height sensor using a 120-GHz FMCW radar, proving the possibility of achieving centimeter accuracy during a full winter season, under different snowpack and environmental conditions, as heavy snowfall. The mmWave technology presents some advantages compared to current commercial devices, as a reliable signal under fresh snow conditions, the possibility of modifying its field of view and a smaller temperature dependence. Additionally, its low hardware requirements (only the generation and detection of LF signals is needed) would allow for the use of low-cost electronics for future versions of the prototype, and the design of a cost-effective snowpack height sensor using mmWave radar technology. The achieved centimeter precision could be improved by calibrating the temperature dependence of the prototype, although the intercomparison with laser and manual measurements shows enough accuracy for most practical purposes.

We have also studied the scattering mmWave-snowpack interaction, concluding that the radar backscattering is mainly affected by the surface properties of the snowpack. We have experimentally found day–night cycles in the intensity of the backscattered radiation, which are caused by variations on the LWC of the uppermost snowpack layer, as demonstrated using numerical simulations. Thus, our measurements and simulations prove that the snowpack surface LWC is the most influential variable on mmWave backscattering properties. Our results are in agreement with the day–night cycles found in the backscattering properties at other frequency ranges and in measurements of brightness temperature of the snowpack [55], [57], [60]. Therefore, we propose the use of the radar sensor not only as an snowpack height sensor, but as a nonperturbative method for measuring the surface LWC.

The microstructure model and the approximate solution of the RTE that we used here to simulate the snowpack backscattering properties were chosen because of their simplicity and ability to qualitatively describe the evolution of the snowpack parameters. However, in order to accurately measure the LWC of the snowpack surface, it will be necessary to introduce more complex models of the snow microstructure and more accurate solving methods for the RTE. Solutions to this problems are already implemented using computationally efficient techniques like the snow microwave radiative transfer (SMRT) model [61].

We have thus shown the possibility of performing long-term measurements of snowpack height and its backscattering coefficient using cost-effective mmWave radar technology. This measurement technology could supplement the currently commercially available technologies. The main strengths of this setup, such as its capability to operate during environmental conditions like heavy snowfall and wind, and the absence of mechanical components complicating maintenance, make the mmWave technology an alternative for the measurement of the snowpack height in remote regions affected by harsh environmental conditions. Therefore, this technology could improve the assessment of snow reserves, thereby supporting more effective hydrological planning, avalanche risk forecasting, and environmental monitoring. Some of its weaknesses, as its slight thermal dependence, could be corrected by calibration and a more complex data processing.

Acknowledgment

The authors would like to thank the Spanish Meteorology Agency (AEMET), especially the observing team from AEMET Aragón Regional Office, for their continuous support on this project, the Ebro River Basin Authority (CHE) for providing data for intercomparison and the Aramón-Formigal Ski Resort for the support offered during the winter season.

References

[1] J. I. López-Moreno and J. M. García-Ruiz, "Influence of snow accumulation and snowmelt on streamflow in the central Spanish pyrenees/influence de l'accumulation et de la fonte de la neige sur les écoulements dans les Pyrénées centrales espagnoles," *Hydrol. Sci. J.*, vol. 49, no. 5, pp. 1–17, Oct. 2004.

[2] R. C. Bales, N. P. Molotch, T. H. Painter, M. D. Dettinger, R. Rice, and J. Dozier, "Mountain hydrology of the western United States," *Water Resour. Res.*, vol. 42, no. 8, pp. 1–19, Aug. 2006.

[3] M. Arenillas, G. Cobos, and J. Navarro, *Datos Sobre La Nieve Y Los Glaciares En Las Cordilleras Españnolas. El Programa ERHIN (1984–2008)*. Madrid, Spain: Ministerio de Medio Ambiente y Medio Rural y Marino, 2008.

[4] L. Holko, L. Gorbachova, and Z. Kostka, "Snow hydrology in central Europe," *Geography Compass*, vol. 5, no. 4, pp. 200–218, Apr. 2011.

[5] J. M. García-Ruiz, J. I. López-Moreno, S. M. Vicente-Serrano, T. Lasanta–Martínez, and S. Beguería, "Mediterranean water resources in a global change scenario," *Earth-Science Rev.*, vol. 105, nos. 3–4, pp. 121–139, Apr. 2011.

[6] J. Magnusson, G. Nævdal, F. Matt, J. F. Burkhart, and A. Winstral, "Improving hydropower inflow forecasts by assimilating snow data," *Hydrol. Res.*, vol. 51, no. 2, pp. 226–237, Apr. 2020.

[7] E. Alfnes, L. M. Andreassen, R. V. Engeset, T. Skaugen, and H.-C. Udnæs, "Temporal variability in snow distribution," *Ann. Glaciol.*, vol. 38, pp. 101–105, Jun. 2004.

[8] J. Revuelto et al., "Meteorological and snow distribution data in the izas experimental catchment (Spanish pyrenees) from 2011 to 2017," *Earth Syst. Sci. Data*, vol. 9, no. 2, pp. 993–1005, Dec. 2017.

[9] H. Zeinivand and F. De Smedt, "Hydrological modeling of snow accumulation and melting on river basin scale," *Water Resour. Manage.*, vol. 23, no. 11, pp. 2271–2287, Sep. 2009.

[10] E. Lastrada, G. Cobos, J. Garzón-Roca, and F. J. Torrijo, "Seasonal variability of snow density in the Spanish pyrenees," *Water*, vol. 13, no. 11, p. 1598, Jun. 2021.

[11] N. Denissova, S. Nurakynov, O. Petrova, D. Chepashev, G. Daumova, and A. Yelisseyeva, "Remote sensing techniques for assessing snow avalanche formation factors and building hazard monitoring systems," *Atmosphere*, vol. 15, no. 11, p. 1343, Nov. 2024.

[12] C. Fierz et al., "The international classification for seasonal snow on the ground," UNESCO, Paris, France, IHP-VII Tech. Documents Hydrol. 83, 2009.

[13] M. P. Bishop, H. Björnsson, W. Haeberli, J. Oerlemans, J. F. Shroder, and M. Tranter, *Encyclopedia of Snow, Ice and Glaciers*. Cham, Switzerland: Springer, 2011.

[14] C. Pielmeier and M. Schneebeli, "Developments in the stratigraphy of snow," *Surveys Geophys.*, vol. 24, no. 5, pp. 389–416, Nov. 2003.

[15] N. J. Kinar and J. W. Pomeroy, "Measurement of the physical properties of the snowpack," *Rev. Geophys.*, vol. 53, no. 2, pp. 481–544, Jun. 2015, doi: 10.1002/2015rg000481.

[16] M. Kodama, K. Nakai, S. Kawasaki, and M. Wada, "An application of cosmic-ray neutron measurements to the determination of the snow-water equivalent," *J. Hydrol.*, vol. 41, nos. 1–2, pp. 85–92, Apr. 1979.

[17] P. Pomerleau et al., "Low cost and compact FMCW 24 GHz radar applications for snowpack and ice thickness measurements," *Sensors*, vol. 20, no. 14, p. 3909, Jul. 2020.

[18] R. Alonso, J. M. G. D. Pozo, S. T. Buisán, and J. A. Álvarez, "Analysis of the snow water equivalent at the AEMet-formigal field laboratory (Spanish pyrenees) during the 2019/2020 winter season using a stepped-frequency continuous wave radar (SFCW)," *Remote Sens.*, vol. 13, no. 4, p. 616, Feb. 2021, doi: 10.3390/rs13040616.

[19] K. G. Kjelgård and T. S. Lande, "Evaluation of UWB radar module for snow water equivalent monitoring," in *Proc. 52nd Eur. Microw. Conf. (EuMC)*, Sep. 2022, pp. 87–90.

[20] F. Koch et al., "Retrieval of snow water equivalent, liquid water content, and snow height of dry and wet snow by combining GPS signal attenuation and time delay," *Water Resour. Res.*, vol. 55, no. 5, pp. 4465–4487, May 2019.

[21] N. Yankielun, W. Rosenthal, and R. E. Davis, "Alpine snow depth measurements from aerial FMCW radar," *Cold Regions Sci. Technol.*, vol. 40, nos. 1–2, pp. 123–134, Nov. 2004.

[22] S. Kolpuke et al., "Airborne multichannel UWB FMCW radar for snow depth measurements," *IEEE Trans. Geosci. Remote Sens.*, vol. 62, 2024, Art. no. 2001918, doi: 10.1109/TGRS.2024.3359125.

[23] M. Tiuri, A. Sihvola, E. Nyfors, and M. Hallikaiken, "The complex dielectric constant of snow at microwave frequencies," *IEEE J. Ocean. Eng.*, vol. JOE-9, no. 5, pp. 377–382, Dec. 1984.

[24] A. H. Sihvola and J. A. Kong, "Effective permittivity of dielectric mixtures," *IEEE Trans. Geosci. Remote Sens.*, vol. GRS-26, no. 4, pp. 420–429, Jul. 1988.

[25] A. D. Frolov and Y. Ya. Macheret, "On dielectric properties of dry and wet snow," *Hydrol. Processes*, vol. 13, no. 1213, pp. 1755–1760, Sep. 1999.

[26] S. G. Warren, "Optical properties of ice and snow," *Phil. Trans. Roy. Soc. A, Math., Phys. Eng. Sci.*, vol. 377, no. 2146, Jun. 2019, Art. no. 20180161, doi: 10.1098/rsta.2018.0161.

[27] J. B. Johnson, "Audibility within and outside deposited snow," *J. Glaciol.*, vol. 31, no. 108, pp. 136–142, 1985.

[28] K. D. Tyagi, A. Kumar, R. Bahl, and K. Singh, "Experimental measurement of acoustic properties in snow," *Acoust. Phys.*, vol. 63, no. 3, pp. 297–301, May 2017.

[29] W. A. Ryan, N. J. Doesken, and S. R. Fassnacht, "Evaluation of ultrasonic snow depth sensors for U.S. snow measurements," *J. Atmos. Ocean. Technol.*, vol. 25, no. 5, pp. 667–684, May 2008.

[30] G. Picard, L. Arnaud, J.-M. Panel, and S. Morin, "Design of a scanning laser meter for monitoring the spatio-temporal evolution of snow depth and its application in the Alps and in Antarctica," *Cryosphere*, vol. 10, no. 4, pp. 1495–1511, Jul. 2016.

[31] S. Ayhan et al., "Millimeter-wave radar sensor for snow height measurements," *IEEE Trans. Geosci. Remote Sens.*, vol. 55, no. 2, pp. 854–861, Feb. 2017, doi: 10.1109/TGRS.2016.2616441.

[32] S. Wielandt et al., "Characterizing snowpack with 60 GHz FMCW millimeter-wave radar sensors," in *Proc. 57th Asilomar Conf. Signals, Syst., Comput.*, Oct. 2023, pp. 1245–1250.

[33] J. C. Wiltse, "History of millimeter and submillimeter waves," *IEEE Trans. Microw. Theory Techn.*, vol. MTT-32, no. 9, pp. 1118–1127, Sep. 1984.

[34] A. M. Niknejad and H. Hashemi, *Mm-Wave Silicon Technology: 60 GHz and Beyond*. Cham, Switzerland: Springer, 2008.

[35] S. T. Buisán et al., "Assessment of snowfall accumulation underestimation by tipping bucket gauges in the Spanish operational network," *Atmos. Meas. Techn.*, vol. 10, no. 3, pp. 1079–1091, Mar. 2017.

[36] R. Nitu et al., "WMO solid precipitation intercomparison experiment (SPICE)(2012–2015)," World Meteorological Organization, Geneva, Switzerland, Instrum. Observing Methods Rep. 131, 2019.

[37] J. Kochendorfer et al., "How well are we measuring snow post-SPICE?" *Bull. Amer. Meteorological Soc.*, vol. 103, no. 2, pp. E370–E388, Feb. 2022.

[38] M. I. Skolnik, *Radar Handbook*. New York, NY, USA: McGraw-Hill, 1970.

[39] I. V. Komarov and S. M. Smolskiy, *Fundamentals of Short-range FM Radar*. Norwood, MA, USA: Artech House, 2003.

[40] M. Jankiraman, *FMCW Radar Design*. Norwood, MA, USA: Artech House, 2018.

[41] Indie Semiconductor FFO GmbH. *Trx 120 067 120-ghz Highly Integrated Iq Transceiver With Antennas in Package in Silicon Germanium Technology*. Accessed: Dec. 20, 2024. [Online]. Available: https://siliconradar.com/products/single-product/120-ghz-transceiver-trx120067/

[42] Y. Tokieda, H. Sugawara, S. Niimura, and T. Fujise, "High precision waterlevel gauge with an FMCW radar under limited bandwidth," in *Proc. Eur. Radar Conf.*, Jan. 2005, pp. 355–358, doi: 10.1109/EURAD.2005.1605633.

[43] S. Ayhan, M. Pauli, T. Kayser, S. Scherr, and T. Zwick, "FMCW radar system with additional phase evaluation for high accuracy range detection," in *Proc. 8th Eur. Radar Conf.*, Oct. 2011, pp. 117–120. [Online]. Available: https://ieeexplore.ieee.org/abstract/document/6101054

[44] K. B. Cooper, R. J. Dengler, N. Llombart, B. Thomas, G. Chattopadhyay, and P. H. Siegel, "THz imaging radar for standoff personnel screening," *IEEE Trans. Terahertz Sci. Technol.*, vol. 1, no. 1, pp. 169–182, Sep. 2011, doi: 10.1109/TTHZ.2011.2159556.

[45] S. Scherr, S. Ayhan, M. Pauli, and T. Zwick, "Accuracy limits of a K-band FMCW radar with phase evaluation," in *Proc. 9th Eur. Radar Conf.*, Oct. 2012, pp. 246–249. [Online]. Available: https://ieeexplore.ieee.org/document/6450702

[46] M. G. Girma et al., "Miniaturized 122 GHz system-in-package (SiP) short range radar sensor," in *Proc. Eur. Radar Conf.*, Oct. 2013, pp. 49–52. [Online]. Available: https://ieeexplore.ieee.org/document/6689110

[47] Indie Semiconductor FFO GmbH. *Collimator Lens*. Accessed: Dec. 20, 2024. [Online]. Available: https://siliconradar.com/datasheets/DatasheetCollimatorLensV1.1.pdf

[48] T. Hauschild and R. Knochel, "Calibration of short range FMCW-radars with network analyzer calibration techniques," in *IEEE MTT-S Int. Microw. Symp. Dig.*, vol. 2, May 1998, pp. 969–972.

[49] J. Barowski, M. Zimmermanns, and I. Rolfes, "Millimeter-wave characterization of dielectric materials using calibrated FMCW transceivers," *IEEE Trans. Microw. Theory Techn.*, vol. 66, no. 8, pp. 3683–3689, Aug. 2018.

[50] S. Thomas, C. Bredendiek, and N. Pohl, "A SiGe-based 240-GHz FMCW radar system for high-resolution measurements," *IEEE Trans. Microw. Theory Techn.*, vol. 67, no. 11, pp. 4599–4609, Nov. 2019.

[51] S. Scherr, S. Ayhan, J. Hofmann, M. Pauli, and T. Zwick, "Sweep time variation algorithm for high accuracy FMCW radar measurements," in *Proc. German Microw. Conf.*, Mar. 2015, pp. 182–185.

[52] D. Long and F. Ulaby, *Microwave Radar and Radiometric Remote Sensing*. Norwood, MA, USA: Artech House, 2015.

[53] Y. Kuga, F. T. Ulaby, T. F. Haddock, and R. D. DeRoo, "Millimeter-wave radar scattering from snow 1. Radiative transfer model," *Radio Sci.*, vol. 26, no. 2, pp. 329–341, Mar. 1991, doi: 10.1029/90RS02560.

[54] B. Wen, L. Tsang, D. P. Winebrenner, and A. Ishimaru, "Dense medium radiative transfer theory: Comparison with experiment and application to microwave remote sensing and polarimetry," *IEEE Trans. Geosci. Remote Sens.*, vol. 28, no. 1, pp. 46–59, Jan. 1990, doi: 10.1109/36.45744.

[55] F. T. Ulaby, T. F. Haddock, R. T. Austin, and Y. Kuga, "Millimeter-wave radar scattering from snow: 2. comparison of theory with experimental observations," *Radio Sci.*, vol. 26, no. 2, pp. 343–351, Mar. 1991, doi: 10.1029/90RS02559.

[56] L. Tsang and J. A. Kong, "Scattering of electromagnetic waves from a dense medium consisting of correlated mie scatterers with size distributions and applications to dry snow," *J. Electromagn. Waves Appl.*, vol. 6, nos. 1–4, pp. 265–286, Jan. 1992, doi: 10.1163/156939392x01156.

[57] S.-E. Shih et al., "Modeling of millimeter wave backscatter of time-varying snowcover—Summary," *J. Electromagn. Waves Appl.*, vol. 11, no. 9, pp. 1289–1298, Jan. 1997, doi: 10.1163/156939397x01160.

[58] P. Bartelt and M. Lehning, "A physical SNOWPACK model for the Swiss avalanche warning: Part I: Numerical model," *Cold Regions Sci. Technol.*, vol. 35, no. 3, pp. 123–145, 2002.

[59] M. Lehning, P. Bartelt, B. Brown, C. Fierz, and P. Satyawali, "A physical snowpack model for the Swiss avalanche warning: Part ii. snow microstructure," *Cold regions Sci. Technol.*, vol. 35, no. 3, pp. 147–167, 2002.

[60] G. Macelloni, S. Paloscia, P. Pampaloni, M. Brogioni, R. Ranzi, and A. Crepaz, "Monitoring of melting refreezing cycles of snow with microwave radiometers: The microwave Alpine snow melting experiment (MASMEx 2002–2003)," *IEEE Trans. Geosci. Remote Sens.*, vol. 43, no. 11, pp. 2431–2442, Nov. 2005.

[61] G. Picard, M. Sandells, and H. Löwe, "SMRT: An active–passive microwave radiative transfer model for snow with multiple microstructure and scattering formulations," *Geosci. Model Develop.*, vol. 11, no. 7, pp. 2763–2788, Jul. 2018.

Víctor Herráiz-López received the B.Sc. degree in physics and the M.Sc. degree in physics and physical technologies from the Sciences Faculty, University of Zaragoza, Zaragoza, Spain, in 2023 and 2024, respectively.

He is currently a full-time Researcher with the Applied Physics Department, University of Zaragoza, and a member with the Photonic Technologies Group, Aragon Institute of Engineering Research (I3A), Zaragoza. His main research interests include radar instrumentation and remote sensing.

Adrián Subías Martín received the B.Sc. degree in physics and the M.Sc. degree in physics and physical technologies from the University of Zaragoza, Zaragoza, Spain, in 2020 and 2021, respectively. He is currently pursuing the Ph.D. degree with the Department of Applied Physics, University of Zaragoza.

He is a member with the Photonic Technologies Group, Aragon Institute of Engineering Research (I3A). His research focuses on radar techniques for snowpack characterization.

Iñigo Salinas received the M.Sc. degree in physics and the Ph.D. degree from the Sciences Faculty, University of Zaragoza, Zaragoza, Spain, in 1996 and 2003, respectively.

He is currently an Associate Professor with the Electrical Engineering and Communications Department, University of Zaragoza, and a member with the Photonic Technologies Group, Aragon Institute of Engineering Research (I3A). His main research interests include multilayers and frequency-selective surfaces on advanced properties glass and optical and radar instrumentation.

Samuel T. Buisán received the M.Sc. and Ph.D. degrees in physics from the University of Zaragoza, Zaragoza, Spain, in 2000 and 2017, respectively.

He is currently the Head of the Observation Department, Spanish Meteorology Agency (AEMET), Madrid, Spain. His research interests include meteorological instrumentation and its operational applications and especially on snow measurements.

Dr. Buisán is a Member of the World Meteorological Organization on different teams such as Global Cryosphere Watch and Surface Measurements.

Rafael Alonso received the M.Sc. and Ph.D. degrees in physics from the University of Zaragoza, Zaragoza, Spain, in 1988 and 1995, respectively.

He is with the Department of Applied Physics, University of Zaragoza, where he is currently a Professor. His research interests include the fields of optical fiber devices, electromagnetic characterization of induction heating systems, optoelectronic instrumentation, and radar technologies.

Dr. Alonso is a Member of the Aragon Institute for Engineering Research (I3A). He is also a Member of the Photonic Technologies Group, University of Zaragoza.